Molecular dynamics simulations of the embedding of a nano-particle into a polymer film

2006 J. Phys.: Condens. Matter 18 2777

(http://iopscience.iop.org/0953-8984/18/10/003)

INSTITUTE OF PHYSICS PUBLISHING JOURNAL OF PHYSICS: CONDENSED MATTER

J. Phys.: Condens. Matter **18** (2006) 2777–2787 doi:10.1088/0953-8984/18/10/003

Molecular dynamics simulations of the embedding of a nano-particle into a polymer film

J G Diaz Ochoa, K Binder and W Paul

Institut für Physik, Johannes Gutenberg Universität, Staudinger Weg 7, D55099 Mainz, Germany

E-mail: Wolfgang.Paul@uni-mainz.de

Received 11 November 2005
Published 20 February 2006
Online at stacks.iop.org/JPhysCM/18/2777

Abstract

In this work we report on molecular dynamics simulations of the embedding process of a nano-particle into a polymeric film as a function of temperature. This process has been employed experimentally in recent years to test for a shift of the glass transition of a material due to the confined film geometry and to test for the existence of a liquid-like layer on top of a glassy polymer film. The embedding process is governed thermodynamically by the prewetting properties of the polymer on the nano-particle. We show that the dynamics of the process depends on the Brownian motion characteristics of the nano-particle in and on the polymer film. It displays large sample to sample variations, suggesting that it is an activated process. On the timescales of the simulation an embedding of the nano-particle is only observed for temperatures above the bulk glass transition temperature of the polymer, agreeing with experimental observations on noble metal clusters of comparable size.

(Some figures in this article are in colour only in the electronic version)

1. Introduction

The dynamic behaviour of polymers in confined geometry as in a film is different from the behaviour in bulk due to the presence of interfaces. Depending on the nature of the interfaces, supported versus free, rough versus smooth, and the strength of the interaction with the support or the solvent (or vacuum) adjacent to a free interface, this change in the dynamics extends to a varying depth into the centre of the film (for reviews see [1, 2]). Consequently, one can find the glass transition in a film to increase (slowing down at both interfaces due to strong interactions [3] and/or corrugation [4]) or decrease (free-standing films [5], smooth supports [6]) to a varying degree. Even for free-standing films the behaviour differs from polymer to polymer [1]. One polymer which showed a very strong suppression of the glass transition in a free-standing film is polystyrene [7], and it has been argued that this can be understood in terms of the existence of a liquid-like layer at the polymer–vacuum (solvent)

interface [7]. In order to obtain information only on the properties of the free film surface, experiments were performed for polystyrene films in which one observes the embedding of clusters of noble metals into the polymer film as a function of temperature. This can be either done with an atomic force microscope for a single metal cluster [8] or by x-ray photoelectron spectroscopy [9] and small-angle x-ray scattering [10] for an ensemble of metal clusters.

The results from these experiments were still inconclusive, partly because the interpretation is also not always straightforward. From the x-ray scattering experiments it was observed that there is a temperature of embedding T_e which is below the glass transition temperature T_g of the film for small clusters, arguing for the existence of a liquid-like layer on top of the film. The difference $T_g - T_e$, however, strongly decreased upon increasing the average size of the clusters [10]. For the interpretation of these findings one has to take into account that this ensemble technique averages over clusters which are not monodisperse. The experiments employed a vapour deposition technique of a submonolayer gold film onto the polystyrene with a subsequent coalescence of gold clusters. Depending on the energy deposited onto the film and the average loading of the surface with gold clusters, one may have a distortion of the equilibrium free surface of the film. Theoretically, it has furthermore been shown that there is a long-ranged interaction between particles adsorbed at a free surface mediated through distortions of the surface [11]. Also from the AFM experiments it was concluded that there is a liquid layer on top of the polystyrene film [8], but the interpretation relied on the oversimplification that below T_g the bulk material is completely frozen. In an analysis of the contact mechanics of the wetting process by which the metal clusters sink into the film, Hutcheson and McKenna [12] could show that the observed time dependence of the height of the nano-particles in the AFM experiment is in perfect agreement with the known viscoelastic and surface tension properties of polystyrene, and that the data can be explained by a T_g suppression by only a few Kelvin without invoking the existence of a liquid layer on top of the film.

The aim of this work is to perform a complementary computer simulation study to the experimental work on the embedding of nano-particles into polymer films upon heating above the glass transition temperature. In section 2 we will define our coarse-grained polymer model for this study. Section 3 will present our results on how to choose a suitable nano-particle model based on a mean-field analysis of the wetting properties of our polymer model onto the nano-particle and on a characterization of the Brownian dynamics of the nano-particle. Section 4 will then discuss our results on the embedding process and relate them to the experimental findings, while section 5 will give a summary and conclusions.

2. Model

We chose to base our work on the well studied bead–spring model introduced by Bennemann *et al* for the study of the glass transition in polymers [13, 14]. The polymer chains are modelled as Lennard-Jones (LJ) beads connected by FENE (finitely extendable non-linear elastic) springs. All beads interact through the LJ potential

$$U_{\mathrm{LJ}}(r_{ij}) = 4\epsilon\left[\left(\frac{\sigma}{r_{ij}}\right)^{12} - \left(\frac{\sigma}{r_{ij}}\right)^{6}\right], \tag{1}$$

where $r_{ij} = |\vec{r}_i - \vec{r}_j|$ is the distance between monomers i and j. Using LJ units defines $\sigma = 1$ as the length unit and $\epsilon = 1$ as the energy unit; we choose the mass of the monomers as $m = 1$, and set the LJ time unit to $\tau_{\mathrm{LJ}} = \sqrt{m\sigma^2/\epsilon}$. The potential is cut and shifted to zero at $r_{ij} = r_c = 2 \times 2^{1/6}\sigma$. Due to our choice of a free surface, we work essentially at zero pressure.

The FENE potential acting between bonded monomers is given as

$$U_{\mathrm{FENE}} = -\frac{kR_b^2}{2}\ln\left[1-\left(\frac{r_{ij}}{R_b}\right)^2\right], \tag{2}$$

with $R_b = 1.5$ and $k = 30$ in LJ units. We have used chains of length $N = 10$ and $N = 50$ for this work.

For this model, the relevant bulk temperature scales at $p = 1$ (in LJ units) are melting temperature $T_{\mathrm{m}} \approx 0.76$ [15], Vogel–Fulcher temperature $T_0 = 0.34$, glass transition temperature $T_{\mathrm{g}} \approx 0.41$ and mode-coupling critical temperature $T_{\mathrm{c}} = 0.45$ [13]. For the zero-pressure case we are investigating here we expect a shift of these temperatures to smaller values as was shown for the pressure dependence of T_{c} in [16]. There it was shown that the mode-coupling critical line fulfilled the relation $\rho(T_{\mathrm{c}})T_{\mathrm{c}}^{-1/4} = 1.27 \pm 0.02$. This model has also been used before to study confinement effects on the glass transition [6, 2]. For smooth, repulsive walls it was shown in this work that the mode-coupling critical temperature of films of the range of thicknesses H we are observing in our simulation, but confined between two walls at $p = 1$, is reduced to $T_{\mathrm{c}}(h) \approx 0.39$–$0.40$.

2.1. Stability of a thin film

To stabilize a thin polymer film we introduce a flat substrate at $z = 0$ attracting the monomers with a 9–3 potential obtained by integrating the LJ interaction over the half space $z < 0$.

$$U_{\mathrm{w}}(z_i) = \epsilon_{\mathrm{H}}\left[\left(\frac{\sigma_{\mathrm{w}}}{z_i}\right)^9 - \left(\frac{\sigma_{\mathrm{w}}}{z_i}\right)^3\right]. \tag{3}$$

We set the distance scale σ_{w} equal to the monomer size $\sigma_{\mathrm{w}} = 1$. The wetting behaviour of our polymer model on such a surface can be tuned by variation of the Hamaker constant, ϵ_{H}, of the interaction potential. For the choice $\varepsilon_{\mathrm{H}} = 3.2$ it is known for our model that there exists a stable polymer film below the wetting temperature $T_{\mathrm{w}} = 1.68$ [17]. We will study a temperature interval $T_{\mathrm{c}} < T < 1.4$, where on the one hand the film is stable and on the other hand the typical relaxation times of the polymer melt are still attainable by simulation.

Choosing a lateral size of the simulation box (with periodic boundary conditions along the x and y directions) of $L = 34.6$ and 1440 chains of length $N = 10$ films of thicknesses ranging from 13 to 17 depending on temperature were obtained. The density in the centre of the film attained typical bulk values between $\rho \approx 0.7$ at high temperature and $\rho \approx 1.0$ at low temperature. A film was prepared using the recoil-growth Monte Carlo method at $T = 0.8$ and then equilibrated at each temperature using a Langevin thermostat.

For the interaction between the nano-particle and the wall we also use the 9–3 form

$$U_{\mathrm{w-np}}(z_{np}) = \epsilon_{\mathrm{w-np}}\left[\left(\frac{\sigma_{\mathrm{w-np}}}{z_{np}}\right)^9 - \left(\frac{\sigma_{w_n p}}{z_{np}}\right)^3\right], \tag{4}$$

with $\sigma_{\mathrm{w-np}} = 1.0$ and $\epsilon_{\mathrm{w-np}} = 3.2$, the same as for the monomers.

The choice of a suitable interaction potential between the monomers and the nano-particle turned out to be a more subtle problem than expected. Since gravity is not important on the distance and mass scales involved, the stabilization of the nano-particle on and in the film is determined by the wetting behaviour of the polymer on the nano-particle. We will discuss in the next section our findings for two versions of the following potential:

$$U_{\mathrm{m-np}}(r_{ij}) = 4\epsilon_{\mathrm{m-np}}\left[\left(\frac{\sigma_{\mathrm{m-np}}}{r_{ij}-R_0}\right)^{12} - \left(\frac{\sigma_{\mathrm{m-np}}}{r_{ij}-R_0}\right)^6\right], \tag{5}$$

where $r_{ij} = |\vec{r}_{\rm np} - \vec{r}_j|$ is the distance between the nano-particle and a monomer in the film. To account for the size difference between the metal clusters we have in mind and the monomers there are two possible choices:

(i) the standard Lennard-Jones form with $\sigma_{\rm m-np} = 4$ and $R_0 = 0$ and
(ii) a modified Lennard-Jones potential with $\sigma_{\rm m-np} = 1$ and $R_0 = 3$

which both lead to an effective nano-particle radius $R_{\rm eff} = 4$ (defined through $U_{\rm m-np}(R_{\rm eff}) = 0$). When we identify the monomer size of our coarse-grained model as $\sigma \approx 4$–5 Å, which is the typical scale found for mapping these models onto chemically realistic ones [18], the nano-particle will have a diameter of 16–20 Å, well comparable with the size of the metal clusters studied in the experiments [9, 10].

3. Stability of the nano-particle on the film

We introduce the nano-particle into the system after equilibration of the polymer film. The particle is 'dropped' onto the film in an equilibration run using a Langevin thermostat. Then the thermostat is switched off so that the nano-particle is thermalized only through the interactions with the polymer film. We therefore expect it to perform a Brownian motion at the surface or in the bulk of the film depending on temperature.

The driving force for the embedding of the nano-particle is the wetting behaviour of the polymer on the particle. A qualitative idea about the wetting (or prewetting [19]) can be obtained in a mean field approach employing the idea of local thermodynamic equilibrium. In this approach, the height of the film on the substrate H as well as of the film on the nano-particle h are given by

$$\mu(H) = \mu(h) = \mu_{\rm coex}(T, p_{\rm coex}), \tag{6}$$

assuming isothermal conditions, where $\mu_{\rm coex}$ is the chemical potential per monomer at coexistence. From hydrostatics we know that

$$\rho \nabla U_{\rm ext} = \nabla P = \rho \nabla \mu, \tag{7}$$

where P is the hydrostatic pressure and where we used the Gibbs law for the last equation. We therefore obtain

$$U_{\rm ext}(H) = \mu_{\rm coex} - \mu_\infty =: \Delta\mu \qquad \text{and} \qquad U_{\rm ext}(h) = \mu_{\rm coex} - \mu_\infty =: \Delta\mu. \tag{8}$$

Here we assume $U_{\rm ext}$ to be given solely by the potential of the wall or the nano-particle, respectively. Eliminating the unknown $\Delta\mu$ we solve for the height of the wetting layer on top of the nano-particle as a function of the equilibrium height of the film observed in the simulation. For the two choices of interaction potential $U_{\rm m-np}$ this gives

$$h = \sigma_{\rm m-np} \left(\frac{2}{1 - \sqrt{1 - \frac{\epsilon_{\rm H}}{\epsilon_{\rm m-np}} \left(\frac{1}{H^3} - \frac{1}{H^9} \right)}} \right)^{1/6} + R_0. \tag{9}$$

For the range of film thicknesses studied in the simulation this is practically identical to

$$h = \sigma_{\rm m-np} \left(\frac{4\epsilon_{\rm m-np}}{\epsilon_{\rm H}} \right)^{1/6} H^{1/2} + R_0. \tag{10}$$

The thickness of the layer on the nano-particle grows as the square root of the film thickness on the flat substrate and both diverge when $\mu_\infty = \mu_{\rm coex}$. A comparison of this prediction for the two choices of nano-particle–monomer interaction is shown in figure 1. For the LJ potential

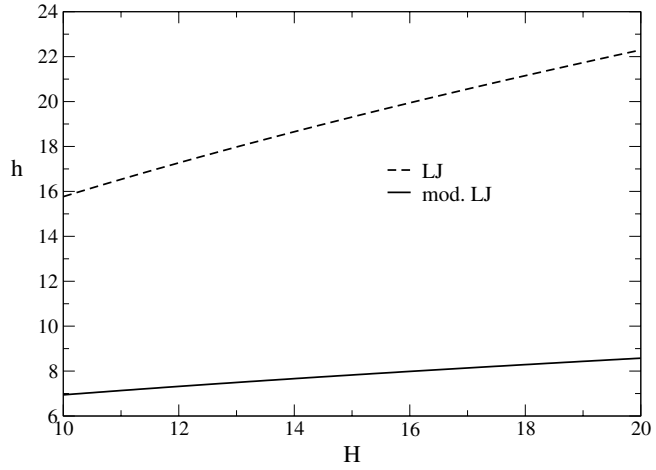

Figure 1. Predictions for the height of the film adsorbed onto the nano-particle in equilibrium as a function of the equilibrium film height on the substrate. The dashed line is for a Lennard-Jones potential with $R_0 = 0$ and $\sigma_{\mathrm{m-np}} = 4$ and the full line for a modified Lennard-Jones potenial with $R_0 = 3$ and $\sigma_{\mathrm{m-np}} = 1$.

this mean-field consideration predicts a film height of $h = 13$–19 on the nano-particle, whereas for the modified LJ it predicts a film height of $h = 7$–9. From this consideration for both choices of potential the nano-particle should experience a driving force embedding it into the film over the whole temperature range studied.

3.1. Brownian motion of the nano-particle

We choose the mass of the nano-particle as $M_{\mathrm{np}} = 25$, so that we expect to be able to observe Brownian motion of the particle in and on the film. As a first check for this expectation we looked at the velocity autocorrelation function shown in figure 2 for the two choices of potential. For the choice of the pure LJ potential we find good agreement with the Ornstein–Uhlenbeck result $\exp\{-\gamma t\}$ where γ is the kinetic friction experienced by the nano-particle, whereas for the modified LJ potential a much faster decorrelation is observed and a pronounced 'cage effect'. The nano-particle bounces within the cage of its first neighbours. A similar result is found for the autocorrelation function of the forces on the nano-particle with both correlation functions showing an initial decay on about one LJ time unit. This difference in decorrelation behaviour can be understood looking at the different shapes of the interaction potentials. The modified LJ potential gives rise to a dense layer of strongly bound monomers at a distance of about $r = 1.2$ from the hard core of the nano-particle, resulting in correlated collisions between the nano-particle and the monomers. For the LJ potential the first neighbour shell is fuzzier, extending from about $r = 4$ to 6, giving rise to mostly two-body collisions.

When one uses a nano-particle adsorbed onto the polymer film as a starting configuration, this difference is first of all enhanced and secondly leads to an instability of the simple LJ particle on the film. For the LJ potential the collisions between the nano-particle and the monomers at the surface of the film are less efficient in thermalizing the nano-particle, and in consequence we found that the particle was not stable on the film but was propelled off the film by collisions with the monomers with a high probability within the simulation time window. From a practical point of view, we therefore found the more realistic modified LJ potential to also be computationally preferable for studying the problem of nano-particle adsorption into a polymer film.

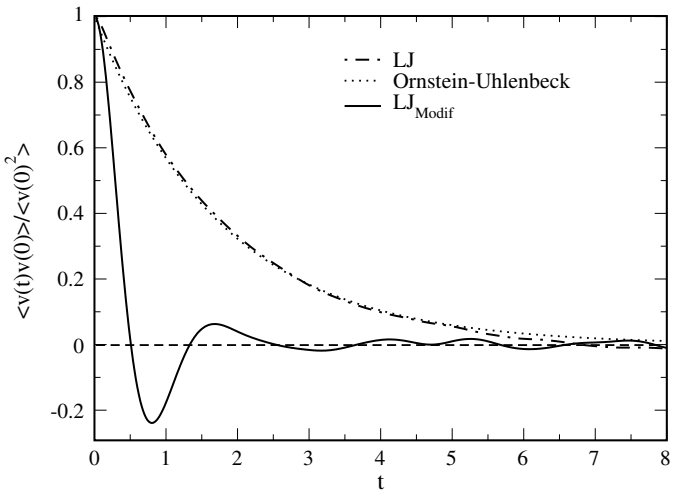

Figure 2. Velocity autocorrelation function for the nano-particle in the polymer film at $T = 1.4$ for the LJ potential (dash–dotted curve) and the modified LJ potential (full curve). The dotted line is a fit with the Ornstein–Uhlenbeck prediction for Brownian motion, giving a kinetic friction $\gamma = 0.56\tau_{\mathrm{LJ}}^{-1}$.

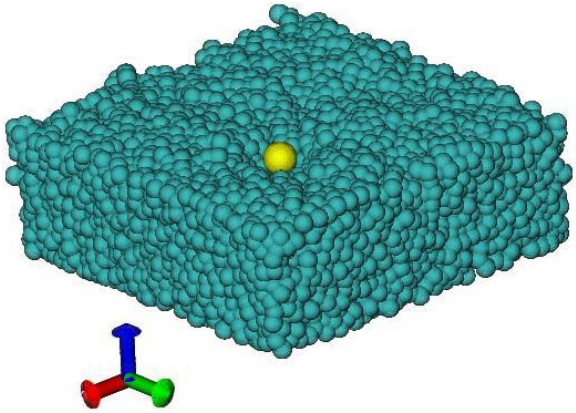

Figure 3. Snapshot of the nano-particle on the film at $T = 0.46$.

4. Results on the embedding process

A typical snapshot of our simulated system is shown in figure 3 for a film made of 1440 chains of length $N = 10$ at a temperature $T = 0.46$. Note that there is a depression like a 'bowl' forming around the nano-particle on the surface of the film. Let us now first turn to the properties of the polymer film we obtained. In figure 4 the density profiles of the monomers as well as that of the nano-particle are shown as a function of the distance z to the substrate for six different temperatures spanning the temperature regime we studied.

For the monomers (full curves) we find a trivial depletion region due to the hard core of the monomers directly at the substrate, followed by a well defined bulk regime and finally a surface regime where the density drops to the vapour phase with a monomer density of zero due to the extremely low vapour pressure of the polymer (we are far below the bulk critical temperature).

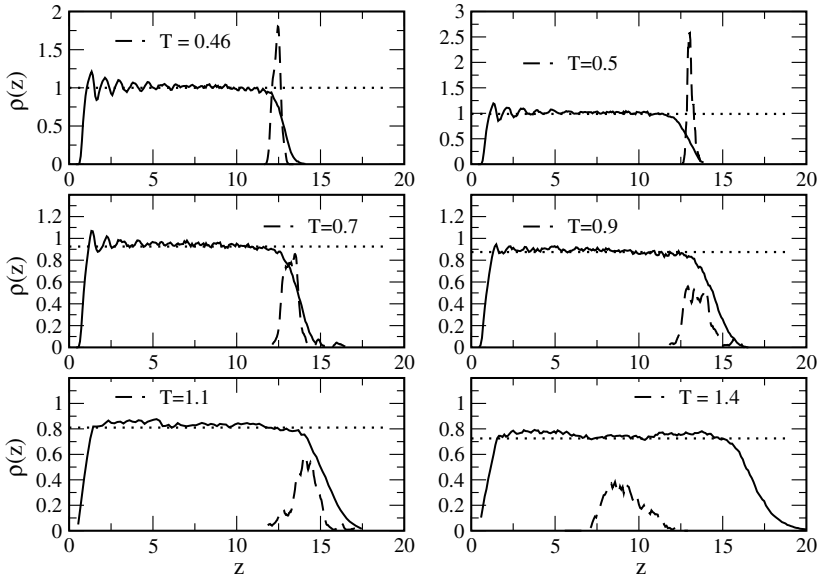

Figure 4. Density profiles as a function of height above the substrate for monomers (full curves) and the nano-particle (dashed curves). Six different temperatures are shown as given in the legends. The dotted lines give the bulk polymer densities at this temperature [17].

The dashed lines give the bulk densities obtained by Müller and McDowell [17], which are well reproduced by the densities in the centre of our polymer films. At low temperatures ($T \leqslant 0.7$) a layering at the substrate sets in, growing in amplitude and extent for the lower temperatures. To analyse the monomer density profiles, we fit them outside the layering regime with the following ansatz:

$$\rho(z) = \rho \frac{1}{2}\left[\tanh\left(\frac{z_0 - z}{w}\right) + 1\right], \tag{11}$$

where ρ is the density in the centre of the film, z_0 is the mean film thickness and w is half the width of the interface. This form reproduces the observed profiles excellently. The results for the film height and interfacial width are presented in figure 5. The mean film thickness increases with temperature—and the density in the centre of the film decreases—according to a constant thermal expansion coefficient

$$\alpha_p = \left(\frac{\mathrm{d}\ln z_0}{\mathrm{d}T}\right)_p = 0.30 \pm 0.01.$$

The width of the interface to the vapour (inset in figure 5) is between two and three particle sizes for all temperatures and the interface sharpens upon cooling the system.

From the measured thermal expansion and our simulation parameters we can calculate the zero-pressure isobar $\rho(T, p = 0)$. Using this result we can try to predict the shift of the relevant temperature scales going from $p = 1$ to 0 by using the empirically found relation [16] $\rho(T_c)T_c^{-1/4} = 1.27 \pm 0.02$. From this we would predict $T_c(p = 0) = 0.35$ compared to $T_c(p = 1) = 0.45$. Scaling the glass transition temperature by the ratio of these values gives an estimate of $T_g(p = 0) \approx 0.32$, which we will use in the following.

Also included in figure 4 is the observed position distribution for the nano-particle (shown by the dashed curves). At $T = 0.46$ and 0.5 the particle is well localized at the film surface,

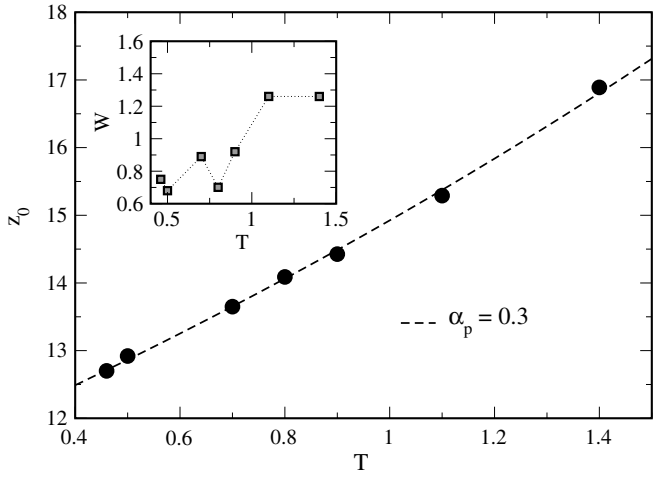

Figure 5. Film thickness as obtained from a hyperbolic tangent fit to the monomer density profile (see text) as a function of temperature. The dashed curve is a fit with a constant thermal expansion coefficient $\alpha_p = 0.30 \pm 0.01$. The inset shows the temperature dependence of the width of the film surface (squares; the line is just a guide to the eye).

around $T = 0.7$ it starts to sink visibly into the film and at $T = 1.4$ it has sunk into the film and its distribution is peaked in the centre of the film. On the timescale of our simulation we therefore observe an embedding of the nano-particle into the film only for temperatures sufficiently larger than T_g.

To compare our findings more quantitatively to experiment we plot in figure 6 the average distance from the nano-particle to the film surface normalized by the size of the nano-particle as a function of temperature normalized by the glass transition temperature. There are three sets of experimental data taken from [10] for different average sizes of the metal clusters formed after vapour deposition. For the smallest size of 9 Å, the experiment found that the clusters had already sunk into the film to an appreciable degree (about two-thirds of their size) at T_g. For the larger clusters the amount of embedding at T_g decreased to one-quarter of the cluster size for 12 Å diameter and practically zero for 17 Å diameter. The last result should be compared to the behaviour of the nano-particle in our simulation as discussed in section 2. Upon heating the system from low temperatures we observe an embedding process slowly starting around T_g, but complete embedding is reached on the simulation timescale only for $T = 1.4 \approx 3.5T_g$. The experimental data do not extend to these high temperatures and also the embedding depth increases much faster with temperature than found in the simulation. We also reversed the temperature sweep in the simulation, starting from the embedded nano-particle at $T = 1.4$ and cooling down the system. A strong hysteresis is observed compared to the heating process and the particle remains embedded to a degree observed in the experiments in the temperature regime close to T_g. We cannot, however, conclude that the level of embedding we are observing along this cooling curve represents an equilibrium measurement. We are still limited by the relatively short simulation times available. The same can be stated, however, for the experimental data. As the discussion by Huntchenson and McKenna [12] clearly showed, the time dependence of the embedding can be described using the known viscoelastic properties of the polymer and the strength of the driving force, i.e., surface tension differences. The timescale for the experiment compared to inherent relaxation times of the polymer is much larger than for the simulation, but also in the experiment, the final state for a metal cluster that

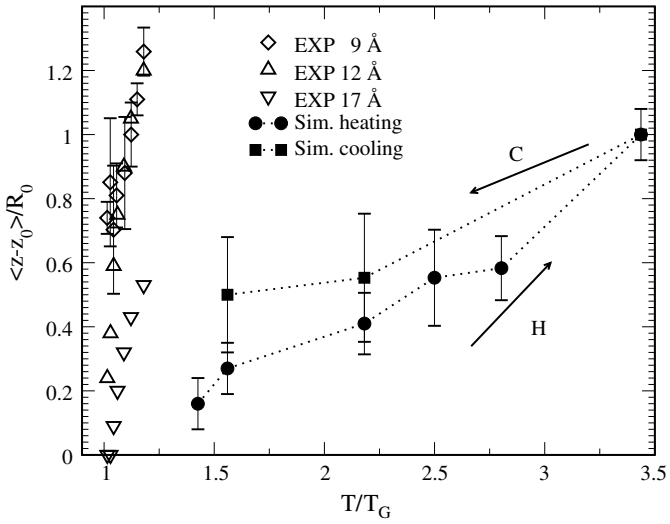

Figure 6. Embedding depth of the nano-particle (full symbols) as a function of temperature. Filled circles are for heating the system starting with a nano-particle adsorbed onto the film; filled squares are for cooling starting with a nano-particle embedded into the film. Open symbols show experimental results for three different average metal cluster sizes obtained by x-ray diffraction [10].

is wetted by the polymer should be complete embedding, which is not reached for the larger clusters on the experimental timescales.

In contrast to the ensemble experiments of [9, 10], the AFM measurements [8] can observe the embedding process for isolated metal clusters. To correctly interpret the observations in these experiments one has to be aware that the embedding process displays elements of metastability, as shown in figure 7. For one of the trajectories the nano-particle sinks into the film at $t \approx 1000\tau_{\mathrm{LJ}}$, for another one this happens around $t \approx 2000\tau_{\mathrm{LJ}}$ and for the five others the nano-particle stays on top of the film for the 4600 time units shown. This is the typical sample to sample variation for a stochastic process which has to surmount a barrier between two states: on top of the film and embedded into the film. One can speculate that this barrier is created by a competition between the surface tension driving the embedding and the line tension of the circumference of the wetted spherical cap of the nano-particle opposing further embedding [12], a situation similar to classical nucleation theory. Typical for such a process, the actual embedding happens on a relatively short timescale compared to the variance between the different embedding times. This large variability of the embedding times necessitates averaging over many embedding processes to obtain a reliable estimate of the average time dependence, a formidable task for the AFM experiments as well as for the simulations, where we are limited to the order of 10 sample paths we can evaluate for selected parameter values only.

5. Conclusions

We have reported on molecular dynamics simulation results of the embedding process of a nano-particle into a polymer film as a function of temperature. The polymer film is modelled using a bead–spring model for which the glass transition has been well studied in the literature before. For the nano-particle/monomer interaction we discussed two possible choices: a simple

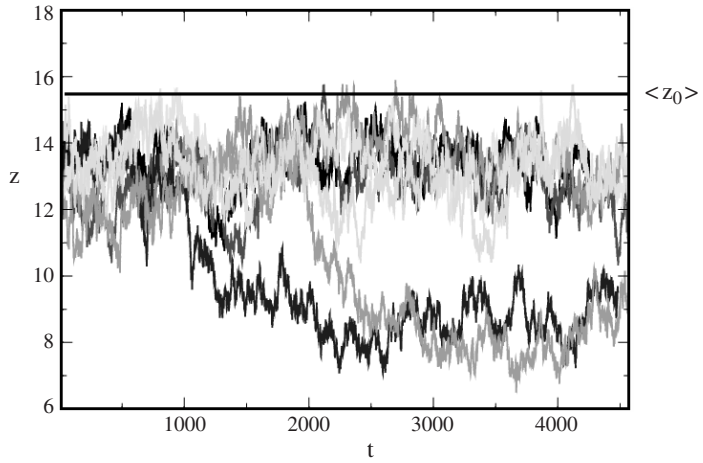

Figure 7. Embedding process as a function of time at $T = 1.2$. Seven realizations of the process are shown, beginning from different starting configurations all with the nano-particle on top of the film. The horizontal line indicates the position of the film surface.

LJ potential with a large interaction range to model the larger size of the nano-particle as compared to the monomers, and a modified LJ potential with a hard core and an interaction range of the same size as the range of the monomer–monomer interaction. For both choices of the interaction a mean-field analysis would predict the formation of a stable wetting layer of the polymer on the nano-particle in the temperature range investigated. This means that there is a driving force for embedding when one starts the simulation with the nano-particle adsorbed onto the polymer film.

In the simulation, the nano-particle is thermalized solely through the collisions with the monomers leading to a Brownian motion of the nano-particle. Here the behaviour we observed was very different for the two choices of potential. The nano-particle with simple LJ potential behaved according to the Ornstein–Uhlenbeck description of Brownian motion, showing an exponential decay of its velocity autocorrelation function. The nano-particle with the modified LJ potential was coupled much more strongly to the monomers due to the much higher density in the monomer layer in contact with the nano-particle. This leads to a liquid-like caging in the velocity autocorrelation function. Due to this stronger coupling, the nano-particle with the modified LJ potential could be stabilized on the polymer film, whereas the one with the simple LJ potential frequently desorbed within the simulation timescale. We therefore performed the studies of the embedding process using the modified LJ potential for the nano-particle. An additional motivation for this choice is that the shorter range of van der Waals interactions is probably closer to reality.

An embedding of the nano-particle into the polymer film was only observable for temperatures above the glass transition temperature of the polymer film, in good qualitative agreement with experimental results on metal clusters of the same relative size compared to the monomers. From our observations there is no indication of the existence of a liquid layer on top of the polymer film exceeding the trivially more mobile interface to the vapour, which is less dense than the bulk of the film and about two to three monomer layers thick. Even at temperatures above T_g the embedding process is very slow, leading to a distinct dynamic hysteresis in the mean observed embedding depending on whether one starts the nano-particle on the surface of the film or in the film. We argued that this kinetic limitation is present in the

experiment as well, although of less importance due to the much longer timescales attainable in the experiment. The embedding process not only takes place on a large average timescale but it also shows a huge variation between different stochastic realizations, typical for an activated process. We conjectured that this could be the manifestation of a competition between difference in surface tensions as the driving force for the embedding and the line tension of the wetted spherical cap on the nano-particle opposing further embedding, leading to a situation similar to classical nucleation theory. With a technique resolving the embedding of a single particle, as in simulation or the AFM experiments, it is therefore very difficult to obtain reliable results on the average time dependence of the embedding process because one would need to average over many realizations.

Acknowledgments

The authors thank M Aichele for providing the program code on which these simulations are based. We acknowledge helpful discussions with M Müller and are grateful for funding by the German Science Foundation with the collaborative research project SFB 625 and the EU Network of Excellence SOFTCOMP.

References

[1] Alcoutlabi M and McKenna G B 2005 *J. Phys.: Condens. Matter* **17** R461
[2] Baschnagel J and Varnik F 2005 *J. Phys.: Condens. Matter* **17** R851
[3] Keddie J L, Jones R A L and Cory R A 1994 *Faraday Discuss.* **98** 219
[4] Smith G D, Bedrov D and Borodin O 2003 *Phys. Rev. Lett.* **90** 226103
[5] Forrest J A, Dalnoki-Veress K, Stevens J R and Dutcher J R 1996 *Phys. Rev. Lett.* **77** 2002
Forrest J A, Dalnoki-Veress K and Dutcher J R 1997 *Phys. Rev.* E **56** 5705
[6] Varnik F, Baschnagel J and Binder K 2002 *Phys. Rev.* E **65** 021507
Varnik F, Baschnagel J and Binder K 2002 *Eur. Phys. J.* E **8** 175
[7] Forrest J A and Dalnoki-Veress K 2001 *Adv. Colloid Interface Sci.* **4** 153
[8] Teichoeb J H and Forrest J A 2003 *Phys. Rev. Lett.* **91** 016104
[9] Zaporojtchenko V, Strunkus T, Erichsen J and Faupel F 2000 *Macromolecules* **34** 1125
Erichsen J, Kanzow J, Schürmann U, Dolgner K, Günter-Schade K, Strunskus T, Zaporojtchenko V and Faupel F 2004 *Macromolecules* **37** 1831
[10] Weber R, Zimmermann K M, Tolan M, Stettner J, Press W, Seeck O H, Erichsen J, Zaporojtchenko V, Strunskus T and Faupel F 2001 *Phys. Rev.* E **64** 061508
Weber R, Grottkopp I, Stettner J, Tolan M and Press W 2003 *Macromolecules* **36** 9100
[11] Oettel M, Dominguez A and Dietrich S 2005 *Phys. Rev.* E **71** 051401
[12] Huntchenson S A and McKenna G B 2005 *Phys. Rev. Lett.* **94** 075103
[13] Bennemann C, Paul W, Binder K and Dünweg B 1998 *Phys. Rev.* E **57** 843
Bennemann C, Baschnagel J and Paul W 1999 *Eur. Phys. J.* B **10** 323
[14] Aichele M and Baschnagel B 2001 *Eur. Phys. J.* E **5** 229
Aichele M and Baschnagel B 2001 *Eur. Phys. J.* E **5** 245
[15] Buchholz J, Paul W, Varnik F and Binder K 2002 *J. Chem. Phys.* **117** 7364
[16] Benneman C, Paul W, Baschnagel J and Binder K 1999 *J. Phys.: Condens. Matter* **11** 2179
[17] Müller M and Macdowell L G 2003 *J. Phys.: Condens. Matter* **15** R609
[18] Binder K, Paul W, Santos S and Suter U W 2004 *Simulation Methods for Polymers* ed M Kotelyanski and D N Theodoru (New York: Dekker) pp 491–510
[19] Gelfand M P and Lipowski R 1987 *Phys. Rev.* B **36** 8725